Extended Lagrangian Formulation of Charge-Constrained Tight-Binding Molecular Dynamics

M. J. Cawkwell,*,[†] J. D. Coe,[†] S. K. Yadav,[‡] X.-Y. Liu,[‡] and A. M. N. Niklasson[†]

[†]Theoretical Division, [‡]Materials Science and Technology Division, Los Alamos National Laboratory, Los Alamos, New Mexico 87545, United States

ABSTRACT: The extended Lagrangian Born–Oppenheimer molecular dynamics formalism [Niklasson, *Phys. Rev. Lett.*, **2008**, *100*, 123004] has been applied to a tight-binding model under the constraint of local charge neutrality to yield microcanonical trajectories with both precise, long-term energy conservation and a reduced number of self-consistent field optimizations at each time step. The extended Lagrangian molecular dynamics formalism restores time reversal symmetry in the propagation of the electronic degrees of freedom, and it enables the efficient and accurate self-consistent optimization of the chemical potential and atomwise potential energy shifts in the on-site elements of the tight-binding Hamiltonian that are required when enforcing local charge neutrality. These capabilities are illustrated with microcanonical molecular dynamics simulations of a small metallic cluster using an sd-valent tight-binding model for titanium. The effects of weak dissipation on the propagation of the auxiliary degrees of freedom for the chemical potential and on-site Hamiltonian matrix elements that is used to counteract the accumulation of numerical noise during trajectories was also investigated.
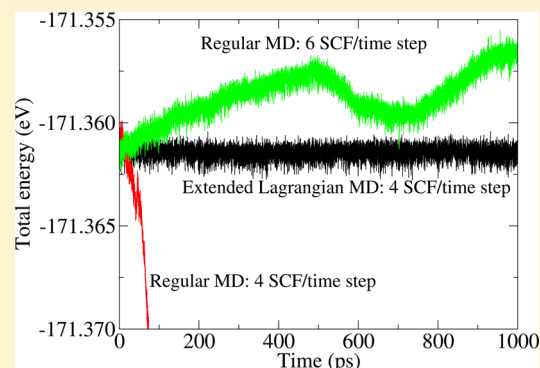
1. INTRODUCTION

Atomistic and molecular dynamics (MD) simulations are powerful tools for the study of phase stability, elasticity, crystal defects, plasticity, fracture, and response to dynamic stimuli in metals. For an overview of many of these applications, see refs 1 and 2. The fidelity of the results of these simulations is controlled mainly by the physical accuracy of the description of interatomic bonding that is used. Models for interatomic bonding based on first principles electronic structure methods such as density functional theory (DFT)[3,4] are usually held as the gold-standard in terms of accuracy. However, the computational expense of first principles methods typically limits their application to relatively small numbers of atoms and short molecular dynamics simulation times. Semi-empirical models, including tight-binding theory, explicitly describe the electronic structure of materials, but they do so from a simplified and parametrized effective single-particle Hamiltonian.[5,6] The use of a small, atom-centered basis and parametrized matrix elements in tight-binding models can lead to a 10^3 to 10^4 speed-up with respect to first principles schemes while maintaining much of the accuracy and transferability that arises from an underlying quantum-based description of the electronic structure.

Electronic structure methods such as density functional theory, Hartree–Fock theory, and their semi-empirical derivatives require the electronic degrees of freedom to be computed self-consistently since the effective single particle Hamiltonian or Fockian itself depends on the charge distribution. The self-consistent field (SCF) optimization takes the form of an iterative series of updates based on mixtures of solutions of the single particle Hamiltonian. When starting from a poor initial guess for the self-consistent charge density or distribution, one may require 15–25 SCF cycles before self-consistency is achieved.

The requirement in Born–Oppenheimer molecular dynamics[7] for computing the interatomic forces at the self-consistent electronic ground state at each time step is a burden on the overall performance since the SCF optimization is computationally very expensive. However, since the difference in the charge density between successive time steps is small, it is customary to obtain a reasonable starting guess for the SCF optimization procedure by extrapolating the charge distributions from previous time steps. While this process can lead to a significant reduction in the number of SCF cycles required at each time step before self-consistency is achieved to within a user-defined tolerance, microcanonical trajectories computed using this procedure exhibit a systematic drift in the total (potential plus kinetic) energy.[8−10] The magnitude of the drift in the total energy can be reduced, although at increased computation cost, by increasing the number of SCF cycles at each time step. The ability to compute accurate microcanonical trajectories underpins the accuracy of simulations in other ensembles[11] and is pivotal for capturing temperature changes arising from, for example, adiabatic compression or endo- or exothermic chemistry.[12,13]

It was shown that the systematic drifts in the total energy seen in Born–Oppenheimer molecular dynamics arise from a

broken time reversal symmetry that is an outcome of the use of charge distributions obtained from the nonlinear SCF optimization in previous time steps as starting guesses for the SCF procedure.[14-16] Time reversal symmetry can be restored in Born−Oppenheimer molecular dynamics through the use of an extended Lagrangian framework from which the starting guesses for the SCF optimization are auxiliary degrees of freedom that are propagated using a time reversible integrator.[15,17,18] Extended Lagrangian Born−Oppenheimer molecular dynamics has been successfully implemented in density functional theory with Gaussian and plane wave basis sets,[19-21] Hartree−Fock theory, and self-consistent charge transfer tight-binding theory (also known as density functional tight binding[22]) with linear scaling electronic structure solvers.[23-25] Here, we demonstrate a new application of the extended Lagrangian Born−Oppenheimer molecular dynamics formalism to a tight-binding model under the constraint of local charge neutrality[6,26-31] where the diagonal (on-site) elements of the tight-binding Hamiltonian are adjusted self-consistently such that every atom is charge neutral. The application of the local charge neutrality boundary condition is a common practice in tight-binding models of materials. It is physically motivated by the short screening distances around charges in metals,[32] and, from a practical point of view, it avoids the unphysical "charge sloshing", that is, wild spatial fluctuations in the electronic density from one SCF to the next, that can arise during self-consistent charge transfer tight binding. The application of local charge neutrality means that the system does not propagate on the regular self-consistent Born−Oppenheimer surface but rather on a constrained Born−Oppenheimer potential energy surface. Nevertheless, the restoration of time reversal symmetry in the SCF procedure using an extended Lagrangian formalism yields the same outcome, namely, a precise conservation of the total energy with a simultaneous reduction in the number of SCF cycles that are required at each time step.

The first extended Lagrangian approach to molecular dynamics most probably goes back to Andersen in 1980,[33] which shortly thereafter was generalized by Parrinello and Rahman.[34] The extended Lagrangian approach was later applied to plane wave *ab initio* molecular dynamics in the Car−Parrinello method in 1985.[35] This method had a significant impact since it, for the first time, allowed more general applications of first principles molecular dynamics simulations based on density functional theory. Other extended Lagrangian formulations of molecular dynamics include, for example, the famous Nosé thermostat from 1984.[36] Extended Lagrangian molecular dynamics has been applied to many problems in atomistic simulations. In electronic structure theory, formulations have typically been direct adaptations of the Car−Parrinello method to different choices of the electronic degrees of freedom.[37-39] In extended Lagrangian Car−Parrinello molecular dynamics, the electronic degrees of freedom are propagated on-the-fly with the nuclei and it does not require an expensive SCF optimization at each time step. However, the dynamics are sensitive to the value of a fictitious electron mass parameter, μ, the time step is often much smaller than those used in Born−Oppenheimer molecular dynamics, and, significantly for this work, the Car−Parrinello method requires a nonvanishing HOMO−LUMO or band gap to work efficiently.[40] Here, we focus solely on a new and practical application of the extended Lagrangian Born−Oppenheimer molecular dynamics formalism that is particularly adapted for

metals. Detailed discussions of the connections between extended Lagrangian Car−Parrinello and extended Lagrangian Born−Oppenheimer molecular dynamics can be found in refs 41 and 42.

In the next section, we outline a general framework for tight-binding models under local charge neutrality, and in Section 3 we give a brief overview of the extended Lagrangian Born−Oppenheimer molecular dynamics formalism. An sd-valent tight-binding model for titanium is described in the Appendix that we apply in extended Lagrangian Born−Oppenheimer molecular dynamics simulations in Section 4. A brief discussion and conclusions are presented in Section 5.

2. TIGHT BINDING UNDER THE CONSTRAINT OF LOCAL CHARGE NEUTRALITY

Tight-binding theory under the self-consistent application of local charge neutrality starts from an effective single particle Hamiltonian, $\mathbf{H}$, that is a sum of the charge independent Slater−Koster Hamiltonian,[5] $\mathbf{H}^0$, and a set of atom-centered potentials, $\mathbf{H}^1$, that self-consistently adjust the electronic occupations such that the set of Mulliken partial charges, $\mathbf{q} = \{q_k\} \rightarrow 0$, that is

$$\mathbf{H} = \mathbf{H}^0 + \mathbf{H}^1 \tag{1}$$

The Slater−Koster Hamiltonian represents the angular and distance-dependent overlap between valence orbitals on neighboring atoms, and the matrix elements of $\mathbf{H}^1$ are

$$H^1_{i\alpha,j\beta} = \Delta H_{i,j} \delta_{i,j} \delta_{\alpha,\beta} \tag{2}$$

where i and j label atoms, α and β label orbitals, $\delta_{i,j}$ is the Kronecker delta, and ΔH is the self-consistently calculated shift in the on-site energy.

In the following, we assume that the set of atomic orbitals is orthogonal, that is, the overlap matrix is equal to the identity matrix. The potential energy is

$$\mathcal{U}(\mathbf{R}, \mathbf{P}) = 2\mathrm{Tr}[\mathbf{PH}] + E_{\mathrm{pair}} \tag{3}$$

where $\mathbf{R} = \{R_k\}$ is the set of atomic coordinates, $\mathrm{Tr}[\mathbf{X}]$ denotes the trace of matrix $\mathbf{X}$, and E_{pair} is a sum of pair potentials that provide strong repulsion at short range and weak attraction at long range. $\mathbf{P}$ is the density matrix computed self-consistently from $\mathbf{H}$ under the condition that

$$2\mathrm{Tr}[\mathbf{P}] = N_e \tag{4}$$

where N_e is the total number of electrons, and $\mathbf{q} = 0$, where

$$q_i = 2 \sum_{\alpha \in i} [P_{i\alpha,i\alpha} - P^0_{i\alpha,i\alpha}] \tag{5}$$

and $\mathbf{P}^0$ is the density matrix for neutral, noninteracting atoms. At finite temperature, the free energy,[20,43] $\mathcal{A}$, is

$$\mathcal{A} = \mathcal{U}(\mathbf{R}, \mathbf{P}) - T_e S(\mathbf{P}) \tag{6}$$

T_e is the temperature of the electronic subsystem, and

$$S(\mathbf{P}) = -2k_B \sum_n [f_n \ln f_n + (1 - f_n) \ln(1 - f_n)] \tag{7}$$

is the electronic entropy where k_B is Boltzmann's constant and f_n is an eigenvalue of the density matrix $\mathbf{P}$, or equivalently the occupation factors of the states

$$f_n = [1 + \exp((\epsilon_n - \epsilon_F)/k_B T_e)]^{-1} \tag{8}$$

where ϵ_n is an eigenvalue of **H** and ϵ_F is the Fermi energy, or chemical potential. The application of an often large, fictitious electronic temperature is a standard method in electronic theory when there is no gap at the chemical potential and/or when interatomic bonds are broken or formed. The use of a finite electronic temperature enables the occupancy of states in the vicinity of the chemical potential to adjust smoothly in response to changes in the nuclear coordinates to maintain a smooth and continuous potential energy surface. We evaluate the set of on-site shifts, $\{\Delta H_{i,i}\}$, in eq 2 via

$$\Delta H_{i,i} = \gamma \sum_{n=1}^{N_{SCF}} (q_i)_n \qquad (9)$$

where N_{SCF} is the number of SCF cycles and $(q_i)_n$ is the value of the Mulliken partial charge on atom i at SCF cycle n.[44] The Hamiltonian **H** is reconstructed at each SCF cycle, and the set of Mulliken partial charges is recalculated using eq 5. The SCF procedure in eq 9 is analogous to an integrating control mechanism that drives the system toward local charge neutrality by either increasing the on-site energies to push charge from each atomic site the net charge $q_i > 0$ or decreasing the on-site energy to draw charge onto the atom if $q_i < 0$. The SCF procedure in eq 9 may be stopped when the magnitude of all of the Mulliken partial charges fall below a user defined tolerance, q_{tol}. In our molecular dynamics simulations, we use either an absolute tolerance, q_{tol}, on the Mulliken partial charges or a user-specified number of SCF cycles per time step. The latter approach is informative since we can compare regular and extended Lagrangian Born–Oppenheimer molecular dynamics at the same level of computational expense. One could achieve precise conservation of the total energy in regular Born–Oppenheimer molecular dynamics if sufficient SCF convergence were achieved, although the computational expense of such a procedure would make this approach impractical for real simulations.

3. EXTENDED LAGRANGIAN QUANTUM-BASED MOLECULAR DYNAMICS

In extended Lagrangian Born–Oppenheimer molecular dynamics, auxiliary electronic degrees of freedom, $\mathbf{h} = \{h_i\}$, are introduced that are constrained to evolve in a harmonic potential that is centered on the self-consistent solution.[18] In self-consistent local charge neutral tight-binding theory, the self-consistently calculated parameters for which good starting guesses are required for the SCF optimization at each time step are the chemical potential (at finite T_e) and $\{\Delta H_{i,i}\}$. This work is a new application of the extended Lagrangian Born–Oppenheimer molecular dynamics formalism since we propagate a potential, the elements of $\mathbf{H}^1$, rather than a charge density. The extended Lagrangian for $\{\Delta H_{i,i}\}$ is

$$\mathcal{L}(\mathbf{R}, \dot{\mathbf{R}}, \mathbf{h}, \dot{\mathbf{h}}) = \frac{1}{2}\sum_{k=1}^{N} m_k \dot{R}_k^2 - \mathcal{U}(\mathbf{R}, \mathbf{P}) + \frac{1}{2}\mu\sum_{k=1}^{N}\dot{h}_k^2$$
$$- \frac{1}{2}\mu\omega^2\sum_{k=1}^{N}(\Delta H_{k,k} - h_k)^2 \qquad (10)$$

where dots denote time derivates, N is the number of atoms, and μ and ω are fictitious mass and frequency parameters for the harmonic potential, respectively. The $\{\Delta H_{i,i}\}$ that enter the extended Lagrangian are the final values obtained from the SCF procedure in eq 9 in the preceding time step. An equivalent

extended Lagrangian is constructed for the chemical potential. The equations of motion are

$$m_i \ddot{R}_i = -\frac{\partial \mathcal{U}(\mathbf{R}, \mathbf{P})}{\partial R_i} - \frac{\mu\omega^2}{2}\frac{\partial}{\partial R_i}\sum_{k=1}^{N}(\Delta H_{k,k} - h_k)^2 \qquad (11)$$

and

$$\mu\ddot{h}_i = \mu\omega^2(\Delta H_{i,i} - h_i) \qquad (12)$$

Upon taking the limit $\mu \to 0$, we recover the regular equations of motion for the atoms

$$m_i \ddot{R}_i = -\frac{\partial \mathcal{U}(\mathbf{R}, \mathbf{P})}{\partial R_i} \qquad (13)$$

and an equation of motion for the auxiliary degrees of freedom

$$\ddot{h}_i = \omega^2(\Delta H_{i,i} - h_i) \qquad (14)$$

both of which can be propagated using a time-reversible Verlet integrator.[45] Equation 13 remains valid even at finite electron temperature provided that the occupancy of the states is described using the Fermi–Dirac distribution since the force derived from the electronic entropy is canceled exactly by the Pulay force that arises at finite T_e.[43]

The power of this approach is that the auxiliary degrees of freedom, **h**, can be used as starting guesses to the SCF optimization at each time step. Since **h** is propagated time-reversibly, the origin of the systematic drift in the total energy in regular quantum-based molecular dynamics is removed. Furthermore, with a sufficiently high value of ω, **h** is always very close to the self-consistent solution such that relatively few SCF cycles are required to reach self-consistency. In the case of the Verlet integrator, the largest curvature of the harmonic wells that also guarantees stability under incomplete SCF convergence is $\omega = 2^{1/2}/\delta t$.[18] We have found that only 1 SCF cycle per time step is required in self-consistent charge transfer tight-binding molecular dynamics.[25]

Since the propagation of the auxiliary degrees of freedom with a time-reversible integrator is lossless, any numerical noise or errors that arise in the calculation of the density matrix will accumulate over time and may eventually lead to the divergence of the trajectory. To counteract the accumulation of numerical noise in the auxiliary degrees of freedom, Niklasson et al.[24,25,46] developed a series of dissipative integration schemes based on a modified Verlet algorithm. The modified Verlet integrators for the auxiliary degrees of freedom at time step t take the form

$$\mathbf{h}_{t+1} = 2\mathbf{h}_t - \mathbf{h}_{t-1} + \delta t^2 \ddot{\mathbf{h}}_t + \alpha\sum_{k=0}^{K} c_k \mathbf{h}_{t-k} \qquad (15)$$

where

$$\ddot{\mathbf{h}}_t = \omega^2(\Delta H_t - \mathbf{h}_t) \qquad (16)$$

and δt is the size of the time step, $\kappa = \delta t^2\omega^2$, α, and the $K + 1$ coefficients c_k are parameters that control the stability and level of the dissipation. These parameters are tabulated in ref 46. The introduction of dissipation via eq 15 breaks time reversal symmetry in the propagation of the auxiliary degrees of freedom. The schemes with small values of K provide the strongest dissipation and break time reversal symmetry to the greatest extent.[24] Similarly, the schemes with large K provide weak dissipation and break time reversal symmetry weakly. The

effect of the dissipation schemes ($5 \leq K \leq 7$) on the stability and systematic drift of the total energy are addressed in Section 4.

4. MICROCANONICAL MOLECULAR DYNAMICS SIMULATIONS OF A SMALL METALLIC CLUSTER

The application of local charge neutrality in the atomistic simulation of metals is attractive since it is both a physically meaningful boundary condition and it provides a relatively straightforward remedy to SCF instabilities and the charge sloshing that arises if the density matrix is computed without constraints on the spatial distribution of charge. In order to illustrate the utility of combining local charge neutrality with the extended Lagrangian Born–Oppenheimer molecular dynamics formalism, we have computed a series of micro-canonical trajectories on a 32 atom metallic cluster in the gas phase. The presence of nonequivalent surface and internal atoms of the cluster give rise to a strong tendency for charge transfer that is removed by the application of the local charge neutrality boundary condition. In fact, in regular self-consistent tight-binding theory, we were not even able to converge the SCF in a static calculation. Hence, it is a challenging test system through which our methods can be assessed but not one that allows a direct comparison between regular self-consistent charge transfer tight-binding theory and a tight-binding model under the local charge neutrality boundary condition. Since our test system is relatively small, we have been able to run relatively long, 1 ns, trajectories in order to assess the long-term accuracy and stability of the extended Lagrangian methods. Periodic test systems without free surfaces would neither give rise to a strong propensity for SCF instabilities and charge sloshing nor allow us to compute the long trajectories required to assess stability. The simulated atomic and electronic structures of the metallic cluster are beyond the scope of this work and are not addressed. We focus our analyses only on the accuracy, long-term stability, and computational expense of the microcanonical molecular dynamics trajectories.

All of our simulations used a time step of $\delta t = 2$ fs and $\gamma = 0.45$ eV/electron in the calculation of $\{\Delta H_{i,i}\}$ via eq 9. The size of the time step is consistent with classical and Born–Oppenheimer molecular dynamics and is much larger than the time steps typically used in Car–Parrinello molecular dynamics.[35] The cluster was created from $2 \times 2 \times 2$ hexagonal close packed (hcp) unit cells that was subsequently relaxed by performing constant temperature molecular dynamics at a temperature of 300 K with a velocity rescaling thermostat for 25 000 time steps. The coordinates and momenta from this simulation were used as the starting condition for a series of 1 ns microcanonical trajectories.

In Figure 1, we present the total energy as a function of simulation time from regular MD trajectories under the local charge neutrality constraint where the starting guesses for the SCF process at each time step are taken as the on-site shifts, ΔH, and Fermi energy from the last SCF cycle of the preceding time step. Here, all of the trajectories exhibit systematic drifts in the total energy that are reduced by increasing the number of SCF cycles in eq 9 at each time step. The dependence of the systematic drift in the total energy on the number of SCF cycles is tabulated in Table 1. The systematic drifts in the total energy seen in these trajectories originate from broken time reversal symmetry in the generation of starting guesses for the SCF procedure at each time step.
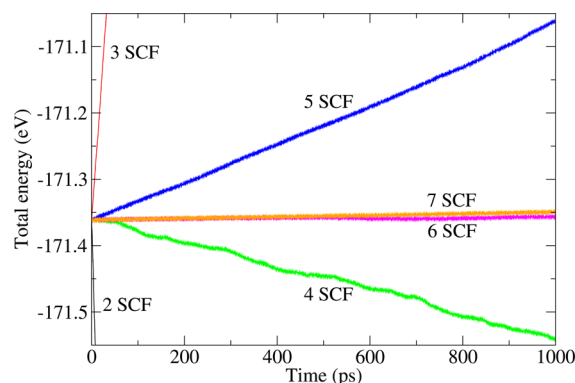

Figure 1. Total energy versus simulation time from regular microcanonical MD simulations with increasing numbers of SCF cycles per 2 fs time step.

Table 1. Systematic Drift in the Total Energy from Regular and Extended Lagrangian Molecular Dynamics Trajectories as a Function of the Number of SCF Cycles Per Time Step[a]

	energy drift (μeV/atom/ps)	
N_{SCF}	regular MD	extended Lagrangian MD
2	−700	−2.2
3	320	−0.078
4	−5.7	<0.0052
5	8.9	<0.0098
6	0.25	<0.00063
7	0.38	<0.0012

[a]The extended Lagrangian trajectories were computed with the dissipation scheme with $K = 5$.

The use of weak dissipation in the propagation of the auxiliary degrees of freedom via eq 15 in extended Lagrangian Born–Oppenheimer molecular dynamics is necessary to ensure the long-term stability of the trajectories. In Figure 2, we plot
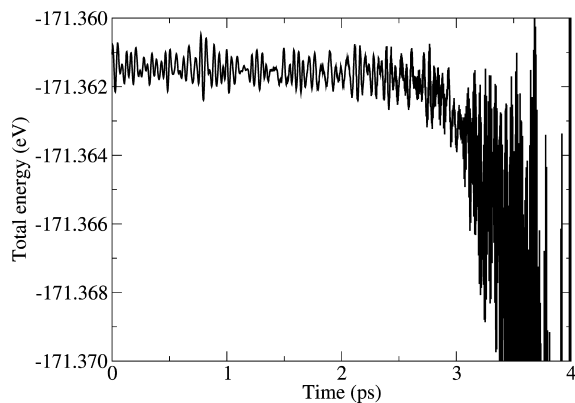

Figure 2. Extended Lagrangian trajectory computed with 3 SCF cycles per time step and no dissipation in the propagation of the auxiliary degrees of freedom.

the total energy as a function of time from an extended Lagrangian trajectory computed with 3 SCF cycles per time step and no dissipation, that is, the auxiliary degrees of freedom were propagated using a regular Verlet integrator. Here, the accumulation of numerical noise caused the trajectory to diverge after only 2.5 ps. Upon the introduction of dissipation in the propagation of the auxiliary degrees of freedom via eq 15,

the extended Lagrangian trajectories exhibit greatly improved long-term stability. However, the strongest dissipation scheme, $K = 3$, which breaks time reversal symmetry to the greatest extent, gives rise to a notable systematic drift in the total energy with 3 SCF cycles per time step that is absent in the schemes with weaker dissipation. The dissipation schemes with $4 \leq K \leq 9$ generated trajectories with almost identical stability and energy conservation.

All of the extended Lagrangian trajectories computed with 3 SCF and dissipation $K > 3$ cycles per time step exhibited a small systematic drift in the total energy. Nevertheless, the magnitude of the energy drifts were about 4 orders of magnitude smaller than those obtained from regular molecular dynamics simulations with 3 SCF cycles per time step and about a factor of 3 smaller than that measured in a regular molecular dynamics trajectory with 6 SCF cycles per time step. The magnitude of the systematic drifts in the total energy in extended Lagrangian Born−Oppenheimer molecular dynamics when 4 or more SCF cycles per time step were used were so small that in Table 1 we can provide only the upper limits. This is illustrated in Figure 3,
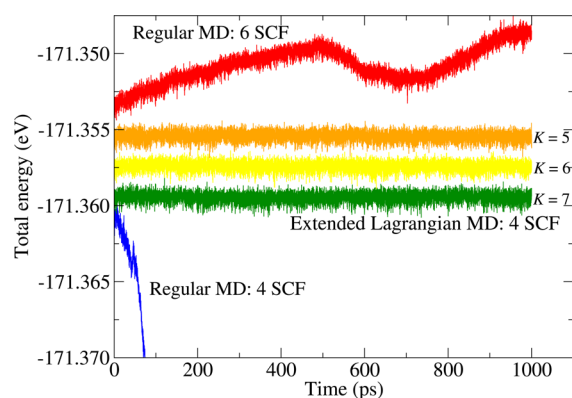

Figure 3. Extended Lagrangian trajectories computed with 4 SCF cycles per 2 fs time step and dissipation schemes $K = 5$, 6, and 7 and regular MD trajectories computed with 4 and 6 SCF cycles per time step. The total energies have each been offset by 0.002 eV for clarity.

where trajectories computed using the extended Lagrangian formalism with 4 SCF cycles per time step and dissipation schemes $K = 5$, 6, and 7 are plotted together with regular Born−Oppenheimer molecular dynamics trajectories computed with 4 and 6 SCF cycles per time step. We consistently observe that the systematic drifts in the total energy from extended Lagrangian Born−Oppenheimer trajectories are at least 4 orders of magnitude smaller than those seen in regular molecular dynamics trajectories with the same number of SCF cycles per time step.

While Table 1 and Figure 3 clearly illustrate that the extended Lagrangian formalism yields vastly improved long-term energy conservation with respect to regular Born−Oppenheimer molecular dynamics at the same computational expense, that is, identical numbers of SCF cycles per time step, it is also informative to study the relative performance of the two schemes when the SCF procedure in eq 9 is instead converged to a user-defined tolerance. In Figure 4a,b, we present the total energy as a function of simulation time for regular and extended Lagrangian Born−Oppenheimer molecular dynamics trajectories where the SCF procedure has been converged such that the magnitude of all of the Mulliken charges are less than $q_{tol} = 10^{-4}$ and 10^{-5} electrons, respectively.
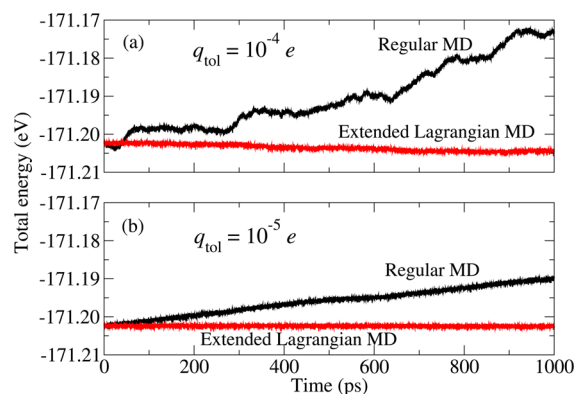

Figure 4. Regular and extended Lagrangian Born−Oppenheimer molecular dynamics trajectories where the SCF procedure has been converged to a tolerance, q_{tol}, on the maximum partial charge on any atom at each time step. (a) $q_{tol} = 10^{-4}$ and (b) $q_{tol} = 10^{-5}$ electrons. The extended Lagrangian trajectories used the dissipation scheme $K = 5$.

The magnitude of the systematic energy drift of the trajectories presented in Figure 4 as well as the average number of SCF per time step required to reach SCF convergence is given in Table 2. The regular Born−Oppenheimer molecular dynamics

Table 2. Systematic Drift in the Total Energy in μeV/atom/ps and the Average Number of SCF Cycles Per Time Step, $\langle N_{SCF} \rangle$, from Regular and Extended Lagrangian Molecular Dynamics Trajectories under an Absolute Tolerance, q_{tol}, on the SCF Convergence at Each Time Step

		regular MD	extended Lagrangian MD
$q_{tol} = 10^{-4}$ electrons	energy drift	0.92	−0.087
	$\langle N_{SCF} \rangle$	4.50	2.95
$q_{tol} = 10^{-5}$ electrons	energy drift	0.38	<−0.0041
	$\langle N_{SCF} \rangle$	6.07	4.07

trajectories exhibit significant systematic energy drifts even under an absolute tolerance on the SCF procedure at each time step owing to the broken time reversal symmetry in the propagation of the chemical potential and $\{\Delta H_{i,i}\}$. Tightening the tolerance on the SCF procedure in regular Born−Oppenheimer molecular dynamics from $q_{tol} = 10^{-4}$ to 10^{-5} electrons decreases the magnitude of the drift by a factor of 2.4 while the mean number of SCF cycles per time step increases from 4.50 to 6.07. The trajectories computed using the extended Lagrangian formalism exhibit significantly smaller energy drifts than the regular Born−Oppenheimer molecular dynamics trajectories. Furthermore, the extended Lagrangian trajectories also require fewer SCF cycles at each time step to converge the Mulliken partial charges to less than q_{tol}, leading to better computational performance. Hence, whether one opts to use a fixed number of SCF cycles per time step or a user-defined tolerance on the SCF procedure, the extended Lagrangian formalism gives rise to significantly improved long-term energy conservation provided that the SCF procedure brings the starting guess to the SCF procedure (the auxiliary degrees of freedom) infinitesimally closer to the self-consistent ground state.

5. CONCLUSIONS

The extended Lagrangian Born−Oppenheimer molecular dynamics formalism has been applied to charge-constrained tight-binding molecular dynamics. The time-reversible propagation of auxiliary degrees for freedom for self-consistently calculated variables, in this case, the on-site shifts in the tight-binding Hamiltonian that remove charge transfer, leads to microcanonical trajectories with greatly improved energy conservation and an overall reduction in the computational expense compared with regular molecular dynamics trajectories. The introduction of weak dissipation in the propagation of the auxiliary degrees of freedom ensures the long-term stability of the trajectories with no discernible effects on the conservation of the total energy.

■ APPENDIX

Tight Binding Model for Titanium

A.1. Density Functional Theory Calculations. The plane wave density functional theory calculations used in the parametrization and testing of our tight-binding model for titanium were performed using the VASP code. We used the generalized gradient approximation exchange correlation functional of Perdew, Burke, and Ernzerhof[47] and projector augmented plane wave potentials.[48,49] A plane wave cutoff energy of 375 eV was used in all calculations. Increasing the plane wave cutoff beyond this value led to no change in the calculated equilibrium lattice parameters of various titanium phases. A fictitious electron temperature corresponding to 0.2 eV was applied in all calculations to improve the convergence of the self-consistent field optimization. The density of the k-point meshes was increased systematically until the total energy had converged to within 0.1 meV/atom.

A.2. Parameterization of Tight-Binding Model. An orthogonal local charge neutral tight-binding model for titanium that shows very good transferability to a number of crystal structures has been developed. Since the d-electron band of Ti has only 2 electrons and it hybridizes strongly with the 3s orbitals, we elected to build the tight-binding model using an sd basis, that is, one s and five d orbitals per Ti atom. The off-diagonal elements of the Slater−Koster Hamiltonian, $\mathbf{H}^0$, are angularly dependent combinations of purely radially dependent bond integrals, $h_{ll'\tau}(R_{ij})$, where R_{ij} is the distance between atoms i and j, l labels the azimuthal quantum number (s, p, d, etc.), and $\tau = \sigma$, π, δ, etc. The diagonal elements of $\mathbf{H}^0$ are equal to the energies of the valence orbitals on isolated atoms, ε_s and ε_d. The radial dependences of the ssσ, sdσ, ddσ, ddπ, and ddδ bond integrals and ε_s and ε_d were parametrized by fitting electronic densities of states computed via a reciprocal space implementation of eq 3 to the densities of states computed using density functional theory for Ti in the face centered cubic (fcc) and body centered cubic (bcc) crystal structures as a function of volume. We represent the radial dependence of the bond integrals by a product of exponentials

$$h_{ll'\tau}(R_{ij}) = h_{ll'\tau}(R_0) \prod_{k=1}^{2} \exp(A_k R_{ij}^k) \qquad (17)$$

where R_0 is a reference bond distance and $\{A_k\}$ are adjustable parameters. Equation 17 is replaced by the polynomial

$$t_{ll'\tau}(R_{ij}) = \sum_{k=0}^{5} B_k(R_{ij} - R_1)^k \qquad (18)$$

to smoothly terminate the bond integrals at a distance $R_{ij} = R_{cut}$. The parameters $\{B_k\}$ are defined by matching the value and first and second derivates of $h_{ll'\tau}$ and $t_{ll'\tau}$ at $R_{ij} = R_1$ and by setting the value and first and second derivates of $t_{ll'\tau}$ to zero at $R_{ij} = R_{cut}$. The parametrization for the five bond integrals is tabulated in Table 3, and the radial dependence of the bond integrals is

Table 3. Parameterization of the Radial Dependences, $h_{ll'\tau}(R_{ij})$, of the Ti−Ti Bond Integrals

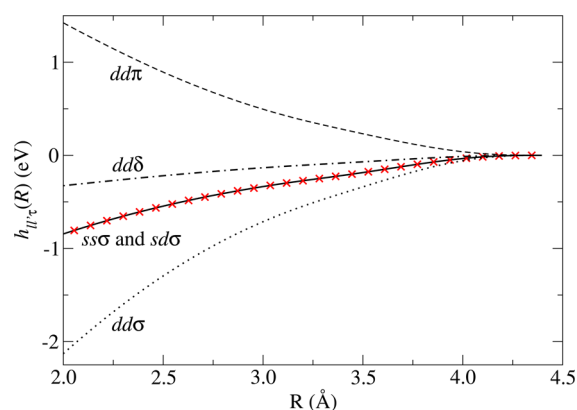| $ll'\tau$	R_0 (Å)	$h_{ll'\tau}(R_0)$ (eV)	A_1 (Å^{-1})	A_2 (Å^{-2})
ssσ	2.89	−0.375	−1.00	−0.10
sdσ	2.89	−0.375	−1.00	−0.10
ddσ	2.89	−0.82	−1.25	−0.20
ddπ	2.89	0.57	−1.25	−0.25
ddδ	2.89	−0.15	−1.05	−0.20

Figure 5. Radial dependences of the Ti−Ti bond integrals, $h_{ll'\tau}(R)$.

presented in Figure 5. The polynomial cutoff tail was added at $R_1 = 3.2$ Å and terminated between second and third nearest neighbors in the hcp lattice at $R_{cut} = 4.4$ Å for each bond integral. The free-atom orbital energies that gave the gave the best fit for the fcc and bcc electronic densities of states were $\varepsilon_s = -5.5$ and $\varepsilon_d = -3.0$ eV.

The densities of states of hcp, fcc, and bcc Ti computed using our tight-binding parametrization and density functional theory are presented in Figure 6, panels a−c, respectively. Owing to
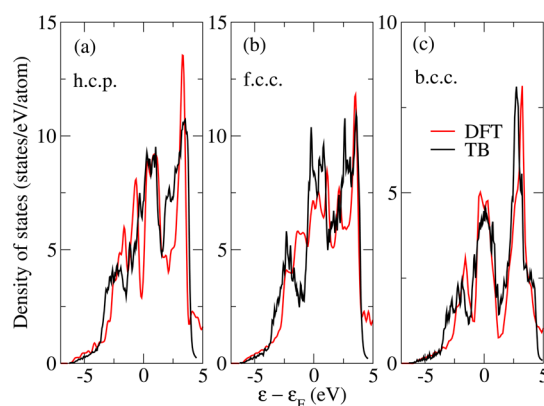

Figure 6. Electronic densities of states for (a) ideal c/a hcp, (b) fcc, and (c) bcc titanium computed via k-space tight-binding and density functional theory.

the small difference in energy between the bcc and close packed phases in Ti we found it to be necessary to reproduce with good fidelity the bcc densities of states as well as the densities of states for the close packed phases in order to achieve a good representation of the phase stability. The electronic densities of states obtained from the orthogonal, sd valent tight-binding parametrization are in excellent agreement with those obtained from density functional theory and suggest that our para-metrization of $\mathbf{H_0}$ is transferable between close packed and more open crystal structures.

The sum of pair potentials

$$E_{\text{pair}} = \frac{1}{2} \sum_{i=1}^{N} \sum_{\substack{j=1 \\ j \neq i}}^{N} \Phi(R_{ij}) \tag{19}$$

was parametrized so that cohesive energies computed from our tight-binding model over a range of volumes match the results of identical calculations performed using density functional theory, that is

$$\mathscr{A}_{\text{DFT}} - \mathscr{A}_{\text{DFT}}^{\text{atoms}} = \mathscr{A}_{\text{TB}} - \mathscr{A}_{\text{TB}}^{\text{atoms}} \tag{20}$$

where $\mathscr{A}^{\text{atoms}}$ is the sum of the free energies of spin polarized isolated atoms,[50] and $\mathscr{A}_{\text{DFT}}$ and $\mathscr{A}_{\text{TB}}$ are the total potential energy obtained from density functional theory and our tight-binding model, respectively. We represent the pair potential by

$$\Phi(R_{ij}) = D_0 \prod_{k=1}^{4} \exp(D_k R_{ij}^k) + E \exp(-FR_{ij}) \tag{21}$$

where $\{D_k\}$, E, and F are fitting parameters. Equation 21 is smoothly terminated at a specified distance using the polynomial function given in eq 18. The pair potential was fitted to density functional theory calculations of the cohesive energy of hcp Ti with $c/a = 1.583$ upon homogeneous dilation of the lattice. Atoms up to and including the third nearest neighbor shell were included in the sum over neighbors in eq 19. The parametrization of eq 21 is provided in Table 4, and its radial dependence is presented in Figure 7.

Table 4. Parameterization of the Pair Potential, $\Phi(R_{ij})$

D_0 (eV)	-2.87809×10^{-6}
D_1 (Å^{-1})	18.3794
D_2 (Å^{-2})	-10.01
D_3 (Å^{-3})	2.41186
D_4 (Å^{-4})	-0.217526
E (eV)	1821.41
F (Å^{-1})	2.65267
R_1 (Å)	6.0
R_{cut} (Å)	7.0

Our model exhibits good transferability between a number of different crystal structures. Energy differences between equilibrium crystal structures, $\Delta\mathscr{A}$, and lattice parameters computed via our tight-binding model and density functional theory are presented in Table 5. The model not only predicts the correct order of structural stability, ω-Ti < hcp < fcc < bcc, but also yields good quantitative predictions for the energy differences. The predicted energy difference between the hcp and fcc structures is within 0.6% of the value calculated using density functional theory. Hence, we can expect our model to give a very good estimate for the energy of the intrinsic stacking fault in hcp Ti. The lattice parameters predicted by the model
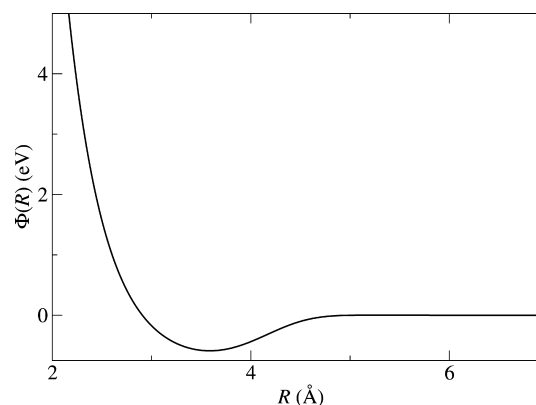

Figure 7. Radial dependence of the Ti–Ti pair potential, $\Phi(R)$.

Table 5. Per Atom Energy Difference in Free Energy Compared with the Optimized hcp Structure, $\Delta\mathscr{A}$, Lattice Parameter, a, and c/a Ratio for the hcp, fcc, bcc, and ω-Ti Crystal Structures from Tight Binding and Density Functional Theory

	$\Delta\mathscr{A}$ (meV/atom)		a (Å)		c/a	
	TB	DFT	TB	DFT	TB	DFT
hcp			2.918	2.922	1.595	1.583
fcc	52.5	52.8	4.104	4.090		
bcc	78.0	100.5	3.250	3.235		
ω-Ti	-7.84	-14.3	4.758	4.551	0.586	0.619

for the hcp, fcc, and bcc structures are in very good accord with values from experiment, $a = 2.951$ Å and $c/a = 1.587$,[51] and/or our density functional theory calculations. The predicted c/a ratio for the hcp structure overestimates the experimental and first-principles calculated values by less than 1%. The lattice parameters predicted for the complex ω-Ti structure deviate from the first-principles calculated values by less than 5%.

■ AUTHOR INFORMATION

Corresponding Author
*E-mail: cawkwell@lanl.gov.

Notes
The authors declare no competing financial interest.

■ REFERENCES

(1) *Atomistic Simulation of Materials: Beyond Pair Potentials*; Vitek, V., Srolovitz, D. J., Eds.; Plenum Press: New York, 1989.
(2) *Handbook of Materials Modeling*; Yip, S., Ed.; Springer: The Netherlands, 2005.
(3) Hohenberg, P.; Kohn, W. *Phys. Rev.* **1964**, *136*, B:864−B871.
(4) Kohn, W.; Sham, L. J. *Phys. Rev.* **1965**, *140*, 1133.
(5) Slater, J. C.; Koster, G. F. *Phys. Rev.* **1954**, *94*, 1498.
(6) Goringe, C. M.; Bowler, D. R.; Hernandez, E. *Rep. Prog. Phys.* **1997**, *60*, 1447−1512.
(7) Wang, I. S. Y.; Karplus, M. *J. Am. Chem. Soc.* **1973**, *95*, 8160.
(8) Remler, D. K.; Madden, P. A. *Mol. Phys.* **1990**, *70*, 921.
(9) Pulay, P.; Fogarasi, G. *Chem. Phys. Lett.* **2004**, *386*, 272.

(10) Herbert, J.; Head-Gordon, M. *Phys. Chem. Chem. Phys.* **2005**, *7*, 3269.

(11) Martinez, E.; Cawkwell, M. J.; Voter, A. F.; Niklasson, A. M. N. *J. Chem. Phys.* **2015**, *142*, 154120.

(12) Cawkwell, M. J.; Sanville, E. J.; Mniszewski, S. M.; Niklasson, A. M. N. *AIP Conf. Proc.* **2012**, *1426*, 1295.

(13) Cawkwell, M. J.; Niklasson, A. M. N.; Dattelbaum, D. M. *J. Chem. Phys.* **2015**, *142*, 064512.

(14) Kolafa, J. *J. Comput. Chem.* **2004**, *25*, 335.

(15) Niklasson, A. M. N.; Tymczak, C. J.; Challacombe, M. *Phys. Rev. Lett.* **2006**, *97*, 123001.

(16) Kühne, T. D.; Krack, M.; Mohamed, F. R.; Parrinello, M. *Phys. Rev. Lett.* **2007**, *98*, 066401.

(17) Niklasson, A. M. N.; Tymczak, C. J.; Challacombe, M. *J. Chem. Phys.* **2007**, *126*, 144103.

(18) Niklasson, A. M. N. *Phys. Rev. Lett.* **2008**, *100*, 123004.

(19) Steneteg, P.; Abrikosov, I. A.; Weber, V.; Niklasson, A. M. N. *Phys. Rev. B* **2010**, *82*, 075110.

(20) Niklasson, A. M. N.; Steneteg, P.; Bock, N. *J. Chem. Phys.* **2011**, *135*, 164111.

(21) Souvatzis, P.; Niklasson, A. M. N. *J. Chem. Phys.* **2014**, *140*, 044117.

(22) Elstner, M.; Porezag, D.; Jungnickel, G.; Elsner, J.; Haugk, M.; Frauenheim, T.; Suhai, S.; Seifert, G. *Phys. Rev. B* **1998**, *58*, 7260.

(23) Sanville, E.; Bock, N.; Niklasson, A. M. N.; Cawkwell, M. J.; Dattelbaum, D. M.; Sheffield, S. Extended Lagrangian Quantum Molecular Dynamics Simulations of Shock-Induced Chemistry in Hydrocarbons, Proceedings of the 14th International Detonation Symposium, Coeur d'Alene, Idaho, April 11–16, 2010; p 91.

(24) Zheng, G.; Niklasson, A. M. N.; Karplus, M. *J. Chem. Phys.* **2011**, *135*, 044122.

(25) Cawkwell, M. J.; Niklasson, A. M. N. *J. Chem. Phys.* **2012**, *137*, 134105.

(26) Sutton, A. P.; Finnis, M. W.; Pettifor, D. G.; Ohta, Y. *J. Phys. C: Solid State Phys.* **1988**, *21*, 35–66.

(27) Sutton, A. P.; Todorov, T. N.; Cawkwell, M. J.; Hoekstra, J. *Philos. Mag. A* **2001**, *81*, 1833.

(28) Horsfield, A. P.; Godwin, P. D.; Pettifor, D. G.; Sutton, A. P. *Phys. Rev. B* **1996**, *54*, 15773.

(29) Horsfield, A. P.; Bratkovsky, A. M.; Fearn, M.; Pettifor, D. G.; Aoki, M. *Phys. Rev. B* **1996**, *53*, 12694.

(30) Finnis, M. *Interatomic Forces in Condensed Matter*; Oxford University Press: Oxford, 2003, p 214.

(31) Girshick, A.; Bratkovsky, A. M.; Pettifor, D. G.; Vitek, V. *Philos. Mag. A* **1998**, *77*, 981.

(32) Pettifor, D. G. *Bonding and Structure of Molecules and Solids*; Oxford University Press: Oxford, 1995, p 194.

(33) Andersen, H. C. *J. Chem. Phys.* **1980**, *72*, 2384.

(34) Parrinello, M.; Rahman, A. *Phys. Rev. Lett.* **1980**, *45*, 1196.

(35) Car, R.; Parrinello, M. *Phys. Rev. Lett.* **1985**, *55*, 2471.

(36) Nosé, S. *J. Chem. Phys.* **1984**, *81*, 511–519.

(37) Hartke, B.; Carter, E. A. *Chem. Phys. Lett.* **1992**, *189*, 358.

(38) Schlegel, H. B.; Millam, J. M.; Iyengar, S. S.; Voth, G. A.; Daniels, A. D.; Scuseria, G.; Frisch, M. J. *J. Chem. Phys.* **2001**, *114*, 9758.

(39) Iyengar, S. S.; Schlegel, H. B.; Millam, J. M.; Voth, G. A.; Scuseria, G.; Frisch, M. J. *J. Chem. Phys.* **2001**, *115*, 10291.

(40) Marx, D.; Hutter, J. *Modern Methods and Algorithms of Quantum Chemistry*, 2nd ed.; Grotendorst, J., Ed.; John von Neumann Institute for Computing: Jülich, Germany, 2000.

(41) Lin, L.; Lu, J.; Shao, S. *Entropy* **2014**, *16*, 110.

(42) Hutter, J. *Wiley Interdiscip. Rev.: Comput. Mol. Sci.* **2012**, *2*, 604.

(43) Niklasson, A. M. N. *J. Chem. Phys.* **2008**, *129*, 244107.

(44) Bowler, D. R.; Miyazaki, T. *Rep. Prog. Phys.* **2012**, *75*, 036503.

(45) Verlet, L. *Phys. Rev.* **1967**, *159*, 98.

(46) Niklasson, A. M. N.; Steneteg, P.; Odell, A.; Bock, N.; Challacombe, M.; Tymczak, C. J.; Holmström, E.; Zheng, G.; Weber, V. *J. Chem. Phys.* **2009**, *130*, 214109.

(47) Perdew, J. P.; Burke, K.; Ernzerhof, M. *Phys. Rev. Lett.* **1996**, *77*, 3865.

(48) Blöchl, P. E. *Phys. Rev. B* **1994**, *50*, 17953.

(49) Kresse, G.; Joubert, D. *Phys. Rev. B* **1999**, *59*, 1758.

(50) Frauenheim, T.; Seifert, G.; Elstner, M.; Hajnal, Z.; Jungnickel, G.; Porezag, D.; Suhai, S.; Scholz, R. *Phys. Status Solidi B* **2000**, *217*, 41.

(51) Wood, R. M. *Proc. Phys. Soc.* **1962**, *80*, 783.